A pulsating heat pipe for space applications: Ground and microgravity experiments

D. Mangini [a], M. Mameli [a, *], A. Georgoulas [a], L. Araneo [c], S. Filippeschi [b], M. Marengo [a, d]

[a] Università di Bergamo, Dipartimento di Ingegnerie e Scienze Applicate, Viale Marconi 5, 24044 Dalmine, BG, Italy
[b] Università di Pisa, DESTEC, Largo Lazzarino 2, 56122 Pisa, Italy
[c] Politecnico di Milano, Dipartimento di Energia, Via Lambruschini 4A, 20158 Milano, Italy
[d] School of Computing, Engineering and Mathematics, University of Brighton, BN2 4GJ Brighton, UK

Received 23 January 2015
Received in revised form
1 April 2015
Accepted 2 April 2015
Available online

1. Introduction

In the last decades the role of two-phase passive heat transfer devices in space thermal control systems gained more and more relevancy because of their lightweight, high performances and reliability. For instance, when heat dissipation rates become very high, heat pipes are preferred to honeycomb structures in radiators panels and they have been widely used to reduce temperature gradients too. The Capillary Pumped Loops (CPL) and Loop Heat Pipes (LHP) technologies have been successfully used as thermal control systems in a large number of missions because of their ability to cover tortuous and longer paths (up to 5 m against gravity, during ground tests) [1]. The ability to transport heat efficiently over long distances is due to the presence of a capillary, or "wick" structure, which is also the more complex and expensive element inside the system.

In order to reduce the effectiveness to cost ratio, more than twenty years ago Akachi [2] introduced an innovative concept of wickless two phase loop, most known as Pulsating Heat Pipe, consisting simply in a small diameter tube or channel, bended in several turns, with alternated heated and cooled zones. The pipe is evacuated and partially filled with a working fluid that resides in the form of liquid slugs and vapor plugs train thanks to the slight predominance, at least in the static condition, of capillary forces with respect to buoyancy forces. The heated vapor plugs expand and push the adjacent fluid towards the cold zone where heat is rejected and vapor condenses, recalling the adjacent fluid back to the evaporator zone. This process results in a chaotic and oscillating fluid motion as well as flow pattern transitions [3], nevertheless, the system is able to reach a pseudo-steady state in a wide range of working conditions [4]. The PHP internal diameter is usually less than the static critical diameter defined as $d_{cr} = 2\sqrt{\sigma/g(\rho_l - \rho_v)}$[5].

* Corresponding author.
E-mail address: mauro.mameli@unibg.it (M. Mameli).

Nomenclature

Bo	bond number [−]
d	diameter [m]
FR	filling ratio [−]
g	gravity acceleration [m/s^2]
Ga	Garimella number [−]
$\dot{Q}$	heat input power [W]
R	thermal resistance [K/W]
Re	Reynolds number [−]
T	temperature [°C]
U	fluid velocity [m/s]
We	Weber number [−]
μ	dynamic viscosity [Pa·s]
ρ	density [kg/m^3]
σ	surface tension [N/m]

Subscripts

Bo	bond number
c	condenser zone
cr	critical
e	evaporator zone
eq	equivalent
Ga	Garimella number
l	liquid phase
max	maximum
min	minimum
Re	Reynolds number
v	vapor phase
We	Weber number

Despite the fact that, in this condition, the capillary forces are strong enough to create an initial slug-plug configuration, gravitational and inertial forces still play a crucial role. When the device is gravity assisted (vertical or bottom heated mode), the flow motion is more vigorous and the thermal performance is higher with respect to the case when the PHP is perfectly horizontal and gravity acceleration is always normal to the main flow path direction [6,7]. It is quite complex to build a PHP, which is gravity-independent on ground, even if some successful attempts of performance independent on orientation have been proposed with three-dimensional layouts [8,9]. In this regard, microgravity experiments are mandatory if one is interested to decouple completely the buoyancy from the inertia effects. By the time being, several experiments in microgravity conditions have been performed: Gu et al. [10] have been the first testing a transparent tube PHP [11] and a Flat Plate PHP in zero gravity conditions, concluding that under reduced gravity the PHP showed better heat transport performance than that under normal and hypergravity. Taking a deep look at their results this assessment is clear only when the device works in top heated mode (i.e. when the evaporator above the condenser). Mantelli et al. [12] provided a similar conclusion testing a planar copper tube PHP (sixteen turns, 1.27 mm I.D.), on a suborbital sounding rocket flight. In order to verify the effect of the gravity field on a perfectly planar PHP both in bottom heated mode and in horizontal position, Mameli et al. [13] tested the dynamic response to the gravity field of a planar copper tube PHP (sixteen turns, 1.1 mm I.D.) filled with FC-72 during the 58th ESA Parabolic Flight Campaign, showing that the horizontal PHP performance was not affected by the gravity field variation occurring during the parabolic trajectories. Furthermore they performed ground tests by tilting the device from the vertical to the horizontal position during operation, showing a clear analogy with the thermal response of the vertical PHP under the transition from hypergravity to microgravity and viceversa. In the bottom heated mode, the PHP never showed a better heat transfer under reduced gravity: the evaporator temperatures tend to increase towards the same values obtained during the horizontal tests on ground.

Both Gu et al. [10] and Mameli et al. [13] illustrated the possibility to build a PHP for space application with an internal diameter bigger than the static critical diameter on ground. Under reduced gravity, body forces are negligible and the threshold diameter to obtain a slug-plug configuration increases. Since the mass of the thermal fluid per unit length is proportional to the square of the I.D, increasing the inner diameter is also beneficial in terms of total heat exchanged. Theoretically for g = 0 m/s^2 the capillary diameter tends to infinite, anyway, the limit to the increase of the inner diameter is also given by inertial and viscous effects, in the sense that when the fluid velocity is high, the menisci are unstable and the slug-plug condition is only possible for smaller diameters with respect to the capillary limit. The dynamic threshold levels, evaluated by means of Weber and Garimella criteria proposed by Mameli et al. [13], $d_{We} \leq 4\sigma/\rho_l U_l^2$ and $d_{Ga} \leq \sqrt{160\mu_l/\rho_l U_l \sqrt{\sigma/(\rho_l - \rho_v)\cdot g}}$, may be more suitable to define the limit for space applications, even if further experimental validations are necessary. In order to provide some order of magnitudes, Table 1 shows the confinement diameters relatively to static and dynamic criteria both in earth and microgravity conditions for FC-72 at 20 °C, assuming a fluid mean bulk velocity of 0.1 m/s and a microgravity level of 0.01 m/s^2, while Fig. 1 shows only the dynamic threshold diameters over fluid temperature.

The aim of the present work is to prove, also by means of a first flow visualization, that a two-phase wickless closed PHP with a diameter bigger than the static critical one on ground can work as a PHP (i.e. slug oscillating flow) under the occurrence of microgravity conditions, opening the frontiers to a new family of Pulsating Heat Pipes only for space applications.

2. Experimental apparatus and procedure

Following the discussion above and the diameter thresholds (Table 1), an aluminum Closed Loop PHP with 3 mm internal diameter filled with FC-72 have been tested at different heat loads (up to 160 W), orientations (BHM, horizontal), transient gravity levels (0 g, 1 g, 1.8 g) during the 61st ESA Parabolic Flight Campaign. The proposed cooling device is made of an aluminum tube (I.D./O.D. 3.0 mm/5.0 mm; Total length: 2.55 m) bended into a planar serpentine with ten parallel channels and five turns at the

Table 1
Confinement diameters for FC-72 at 20 °C accordingly to static and dynamic criteria.

FC-72 @ 20 °C	d_{cr} [mm] (static)	d_{Ga} [mm] (U_l = 0.1 m/s)	d_{We} [mm] (U_l = 0.1 m/s)
Earth g = 9.81 m/s^2	1.68	0.75	2.79
Microgravity g = 0.01 m/s^2	52.88	4.23	

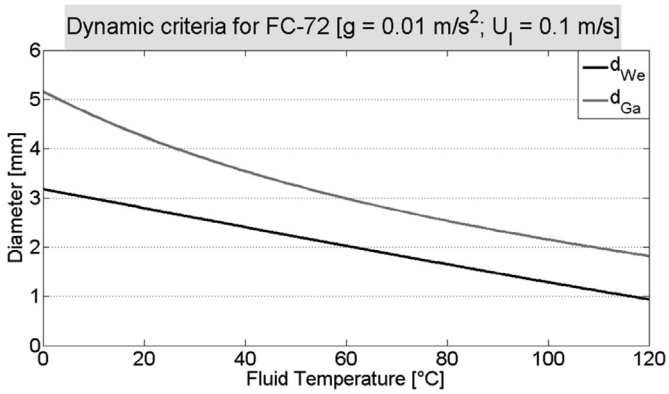

Fig. 1. Dynamic threshold diameters for FC-72 for different fluid temperatures evaluated at an average bulk velocity of the fluid equal to 0.1 m/s and a microgravity level of 0.01 m/s^2.

evaporator (all curvature radii are 7.5 mm), as shown in Fig. 2a. Two "T" junctions allow to close the serpentine in a loop and to derive two ports at each side: one hosts a pressure transducer (Kulite®, XCQ-093, 1.7 bar A), while the second one is devoted to the vacuum and filling procedures. The working fluid is FC-72 and the volumetric filling ratio is 0.5 corresponding to 8.3 ml. The PHP external tube wall is equipped with sixteen "T" type thermocouples (bead diameter 0.2 mm), with an accuracy of ±0.2 K after calibration: ten located in the evaporator zone and six in the condenser zone, as illustrated in Fig. 2a. One additional thermocouple is utilized to measure the ambient air temperature. A glass tube fixed between the two "T" junctions, allows the flow pattern visualization in the top of the condenser zone and it also closes the loop. The device, the "T" junctions and the glass tube are sealed together, by applying a low vapor pressure glue (Varian Torr Seal®).

Fig. 2b shows an exploded view of the test cell, highlighting all its main components. In order to record the fluid dynamics, a compact camera (Ximea®, MQ013MG-ON objective: Cosmicar/Pentax® C2514-M) is positioned behind the PHP by means of an aluminum plate. Due to space restrictions, an inclined mirror is also utilized to reach the desired field of view. Diminishing the region of interest solely at the glass tube, the camera acquires up to 450 fps, with a resolution of 1280 × 200 pixel. The aluminum tube is firstly evacuated by means of an ultra-high vacuum system (Varian® DS42 and TV81-T) down to 0.3 mPa and then it is filled up with the working fluid (FC-72). The working fluid is firstly degased within a secondary tank, by continuous boiling and vacuuming cycles as described by Henry et al. [14]. The aluminum tube is finally filled with a volumetric ratio of 0.5 ± 0.03 and permanently sealed, by

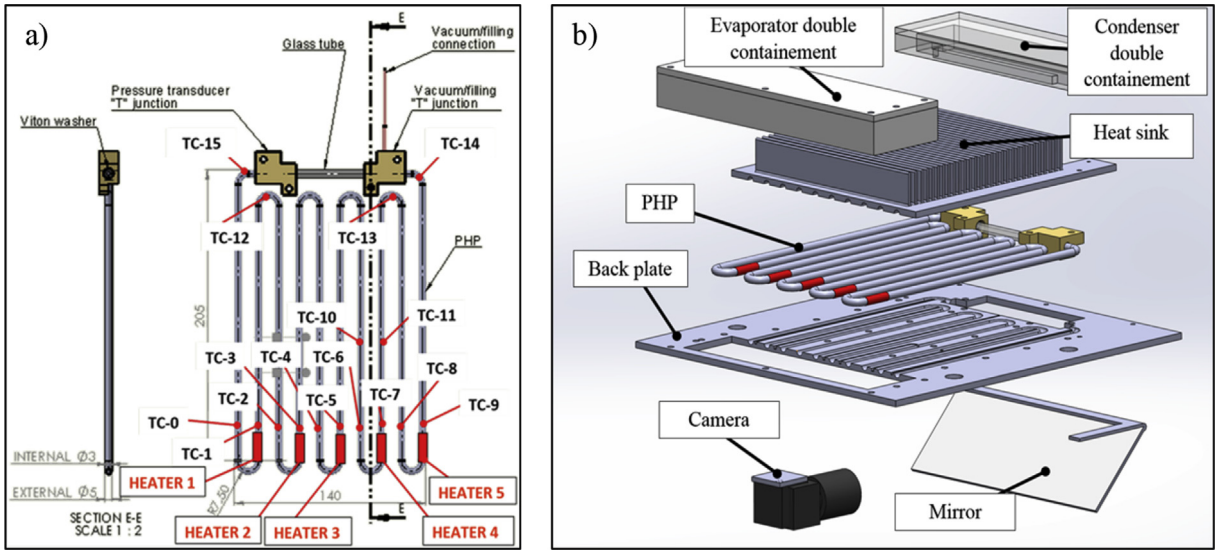

Fig. 2. a) Thermocouples and heaters location along the PHP tube; b) The test cell with all its components.

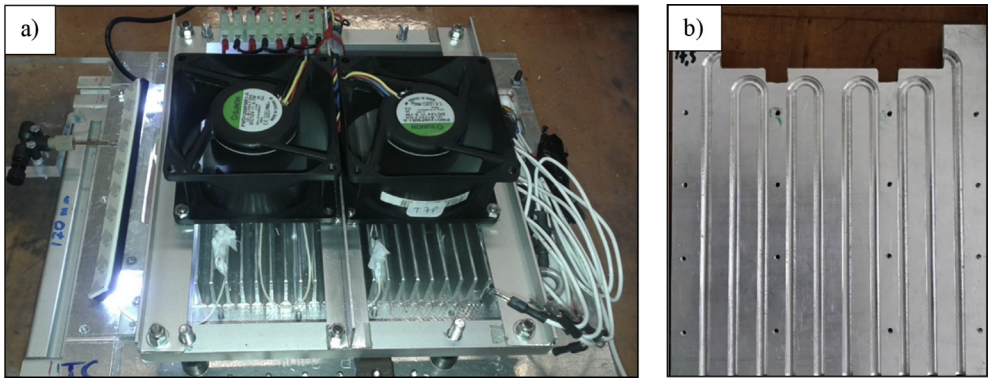

Fig. 3. a) Air fan system mounted above the heat sink; b) Milled heat sink.

Table 2
Heat power input levels set up for ground tests.

Heat power input levels	
Vertical (bottom heated)	Horizontal orientation
10 W	10 W
20 W	20 W
30 W	30 W
40 W	40 W
80 W	50 W
120 W	60 W
160 W	80 W

means of tin soldering. The difference between the actual fluid pressure inside the tube and its saturation pressure, at the ambient temperature, gives an indication of the incondensable gas content (less than 6 PPM).

The device is equipped with five electrical heaters (Thermocoax® Single core 1Nc Ac, 0.5 mm O.D., 50 Ω/m, each wire is 720 mm long) wrapped just above the evaporator U-turns (Fig. 2a) covering a tube portion of 20 mm and providing an asymmetric heating on the device. The parallel assembly of the heaters is connected with a power supply (GWInstek® 3610A) that can provide an electric power input up to 160 W, corresponding to a wall to fluid radial heat flux up to 17 W/cm^2. Due to the low thermal inertia of the heating system, the pseudo steady state condition can be reached in approximately 3 min. The condenser section is 165 mm long and it is embedded into a heat sink, which is cooled by means of two air fans (Sunon® PMD1208PMB-A), as shown in Fig. 3a. In order to optimize the thermal contact, circular cross section channels are milled on both the heat sink and the back plate (Fig. 3b).

These elements are covered by heat sink compound (RS® Heat Sink Compound) before assembling. The ambient temperature is kept constant to 20 °C ± 1 °C during the tests. A three-axis g-sensor (Dimension Engineering®, DE-ACCM3d) is utilized in order to detect the gravity variations during each parabola. The cooling device, the thermocouples, the pressure transducer, the g-sensor, the heating and cooling system as well as the visualization system are placed on a beam structure by means of four anti-vibration bushes. All these components apart from the g-sensor can be orientated both horizontally and vertically (bottom heat mode).

A data acquisition system (NI-cRIO-9073®, NI-9214®, NI-9215®) records the output of the thermocouples, the pressure transducer and the g-sensor and all signals are recorded at 10 Hz. The high-speed camera is connected to an ultra-compact PC (NUC® Board D54250WYB) able to store the images up to 450 fps.

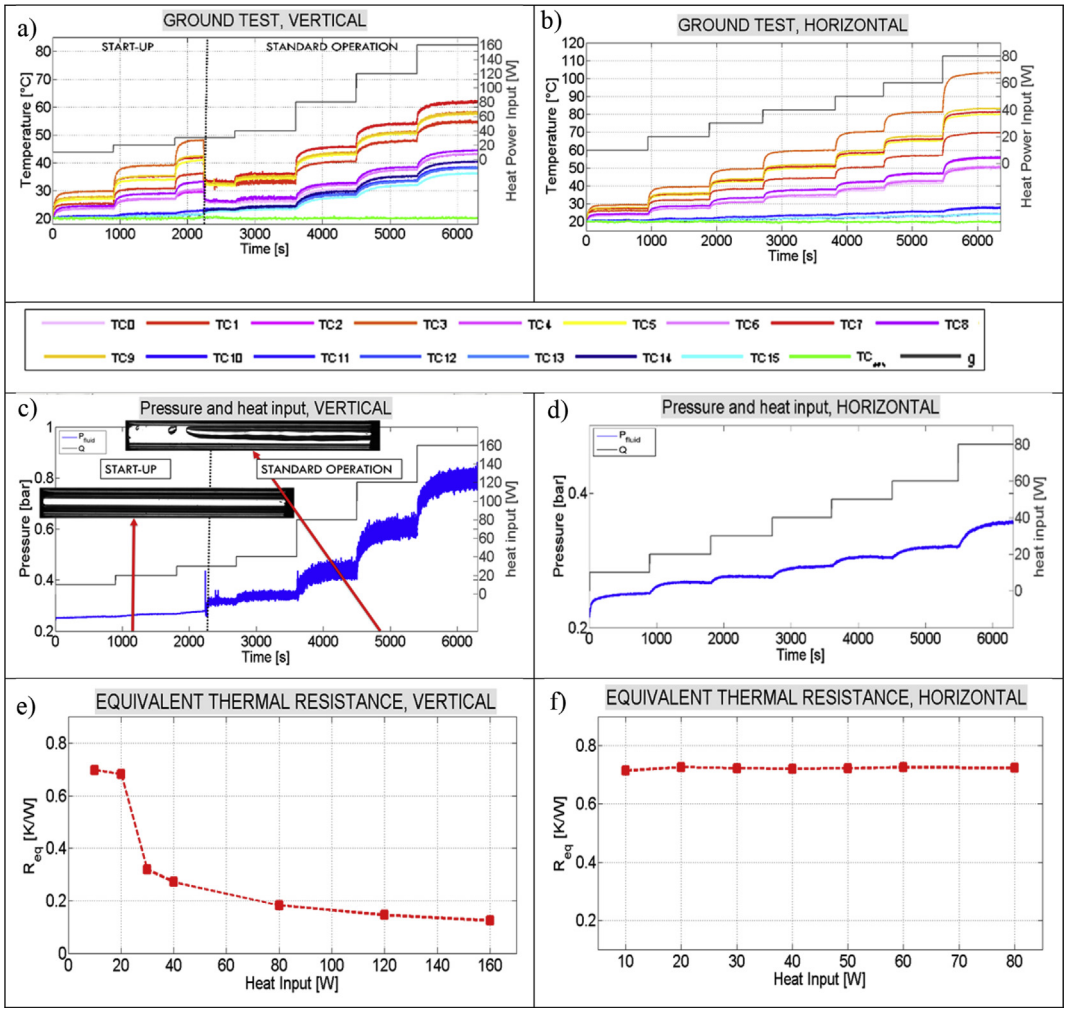

Fig. 4. Temperature temporal evolutions, pressure temporal evolutions and equivalent thermal resistance during thermal characterization on ground, first column: vertical operation, second column: horizontal operation.

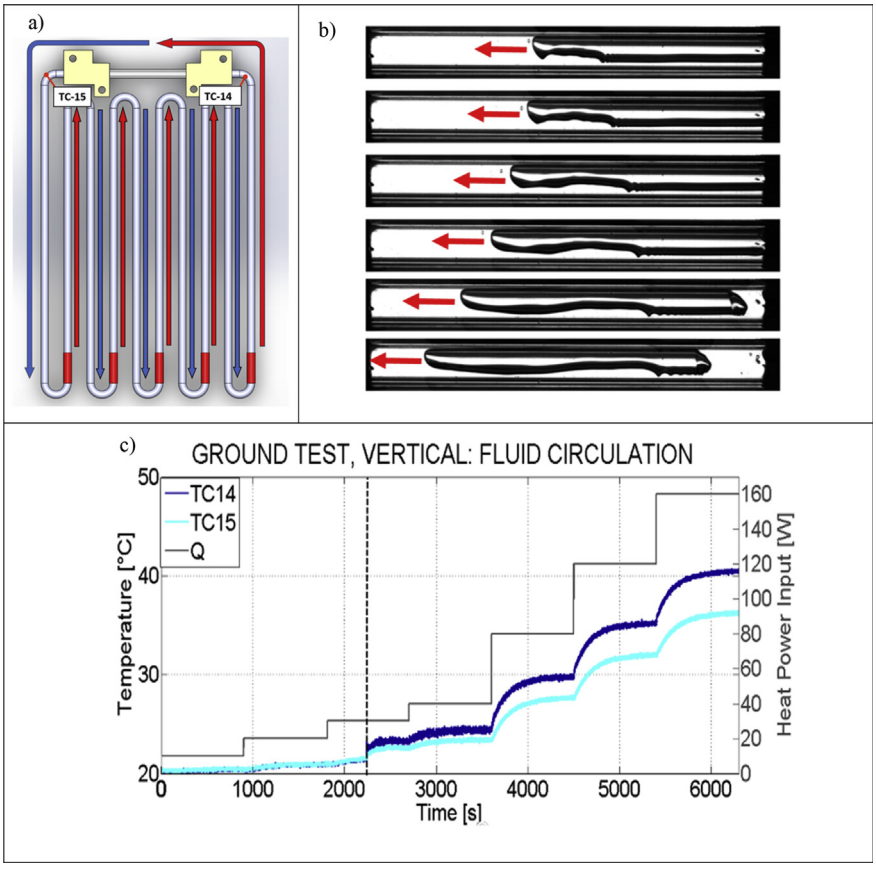

Fig. 5. Fluid net circulation during the vertical tests: a) fluid direction; b) flow visualization (100 fps); c) temperatures at the edges of the glass tube.

The experimental parameters are:

- The heat input level: from 10 W to 160 W for the bottom heat mode orientation and from 10 W to 80 W for the horizontal orientation.
- The gravity field: Normal gravity (1 g) during the test on ground and during the straight flight trajectory; hyper-gravity (1.8 g) before and after the parabola during the ascending and descending maneuvers (duration: 20–25 s each); microgravity during the parabola (duration: 20–21 s).
- The orientation: Bottom Heated mode (BHM) and horizontal position.

The measured quantities are:

- Tube wall temperatures: 10 measuring points in the evaporator zone, 6 in the condenser zone and 1 measuring point that monitors the ambient air temperature.

Table 3
Heat power inputs during flight days.

Flight test procedure		
Parabola N.	PF-I (vertical)	PF-II (horizontal)
Parabola 0	10 W	10 W
From 1 to 5	20 W	20 W
From 6 to 10	30 W	30 W
From 11 to 15	40 W	40 W
From 16 to 20	80 W	50 W
From 21 to 25	120 W	60 W
From 26 to 30	160 W	80 W

- Local fluid pressure in the condenser zone.
- Acceleration: the gravity field variation during each parabola is monitored by means of a three-axis accelerometer.

In addition, a video (80 s at 450 fps) is recorded during each parabola, starting 10 s before the maneuver and stopping around 10 s after the second hyper-gravity period.

Supplementary video related to this article can be found at http://dx.doi.org/10.1016/j.ijthermalsci.2015.04.001.

3. Experimental results

In the present section, results are presented in terms of temperature and pressure temporal evolutions while images of the flow pattern within the condenser zone are also illustrated. The red/yellow lines indicate the temporal evolution of the temperatures in the evaporator zone just above the heater (TC1, TC3, TC5, TC7, TC9); the pink color variations correspond to the temperatures at the evaporator zone far from the heaters (TC0, TC2, TC4, TC6, TC8); the temperatures recorded in the condenser zone are illustrated with blue color variations (TC10, TC11, TC12, TC13, TC14, TC15), while the ambient temperature is visible in green. To mention is that the secondary y-axis at the right corresponds to the heat input levels during the thermal characterization on ground, and the gravity acceleration in case of flight tests.

The overall equivalent thermal resistance is evaluated at each heat input step by the following equation.

$$R_{eq} = \Delta\overline{T}_{e-c} \Big/ \dot{Q} \tag{1}$$

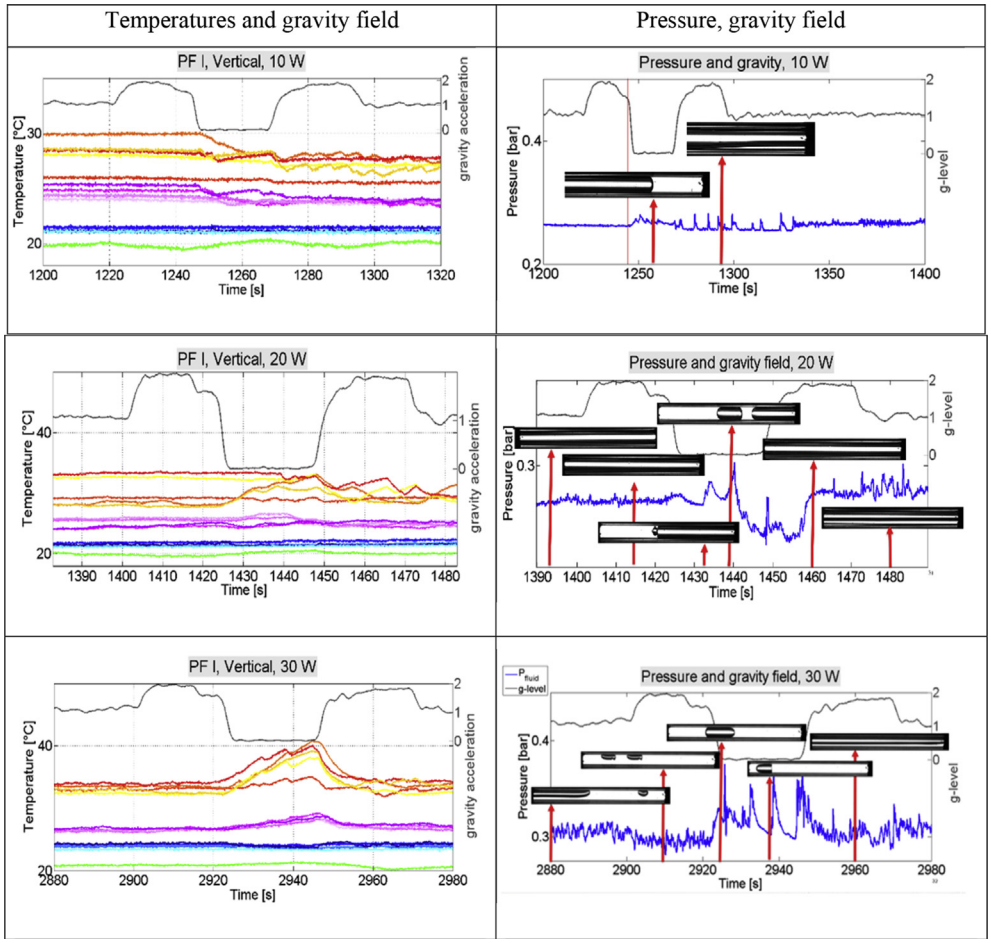

Fig. 6. Flight tests in vertical position, first column: temperatures and gravity field; second column: pressure and gravity field, in conjunction with visual images (red arrows identify the exact timing of each image). (For interpretation of the references to color in this figure legend, the reader is referred to the web version of this article.)

where $\Delta\overline{T}_{e-c}$ is the difference between the evaporator and the condenser average temperatures in the pseudo-steady state, and $\dot{Q}$ is the effective heat power input provided to the evaporator zone.

3.1. Ground tests

The device has been thermally characterized on ground (earth gravity conditions) in vertical (BHM: bottom heated mode) and in horizontal orientation with heat power input levels up to 160 W and 80 W respectively, for a duration of 15 min in each power input step (see Table 2).

In the vertical position the device works as a Closed Loop Two Phase Thermosyphon (TS mode) where the fluid circulation can be obtained from the bubble lift principle defined by Franco et al. [15] which is explained thoroughly in the next section.

3.1.1. Bottom heated mode (BHM)

In the vertical position, two different working modes can be recognized: (i) the start-up and (ii) the standard operation [3]. During the start-up, the heat input up to 30 W is not sufficient to pump the fluid batches up to the condenser zone. The liquid phase remains relegated in the evaporator section, and no fluid motion can be identified in the condenser zone, since the pressure readings do not exhibit any fluctuations and the transparent tube section appears completely dry (Fig. 4c). As a consequence, the higher the heat power input, the higher the temperatures in the evaporator zone (Fig. 4a), and the equivalent thermal resistance reaches approximately 0.7 K/W (Fig. 4e) during the start-up. When the heat power input is set at 40 W, the higher pressure reached in the evaporator zone is sufficient to pump the liquid batches in the condenser zone: the pressure signals shows suddenly vigorous fluctuations and a slug/plug flow is observed in the transparent horizontal section (Fig. 4c). Therefore, the heat exchange is enhanced by convection, the equivalent thermal resistance decreases, arriving at 0.1 K/W at 160 W of heat power input (Fig. 4e), without any thermal crisis.

Furthermore, the asymmetrical position of the heaters has a direct effect on the fluid motion. In the heated branches (up-headers) the fluid batches are lifted up from the evaporator to the condenser in the form of non-coherent slugs, by means of the expanding vapor bubbles; along the adjacent branches (down-comers) the gravity head assists the return of the fluid from the condenser down to the evaporator zone, as shown in Fig. 5a. The alternation of up-headers and down-comers generates a fluid motion in a preferential direction, activating a net circulation. Temperatures at the edges of the transparent section are equal during the start-up, because there is no fluid motion. However, as soon as the fluid starts to reach the condenser zone, TC 14 starts to show higher values than TC 15 (Fig. 5c). The fluid that is pumped from the up-header, releasing thermal energy during its passage through the T-junctions and the transparent section, reaches the other end with a lower temperature. This can also be observed through the transparent section of the condenser that connects directly the up-header and the down-comer at the right and left

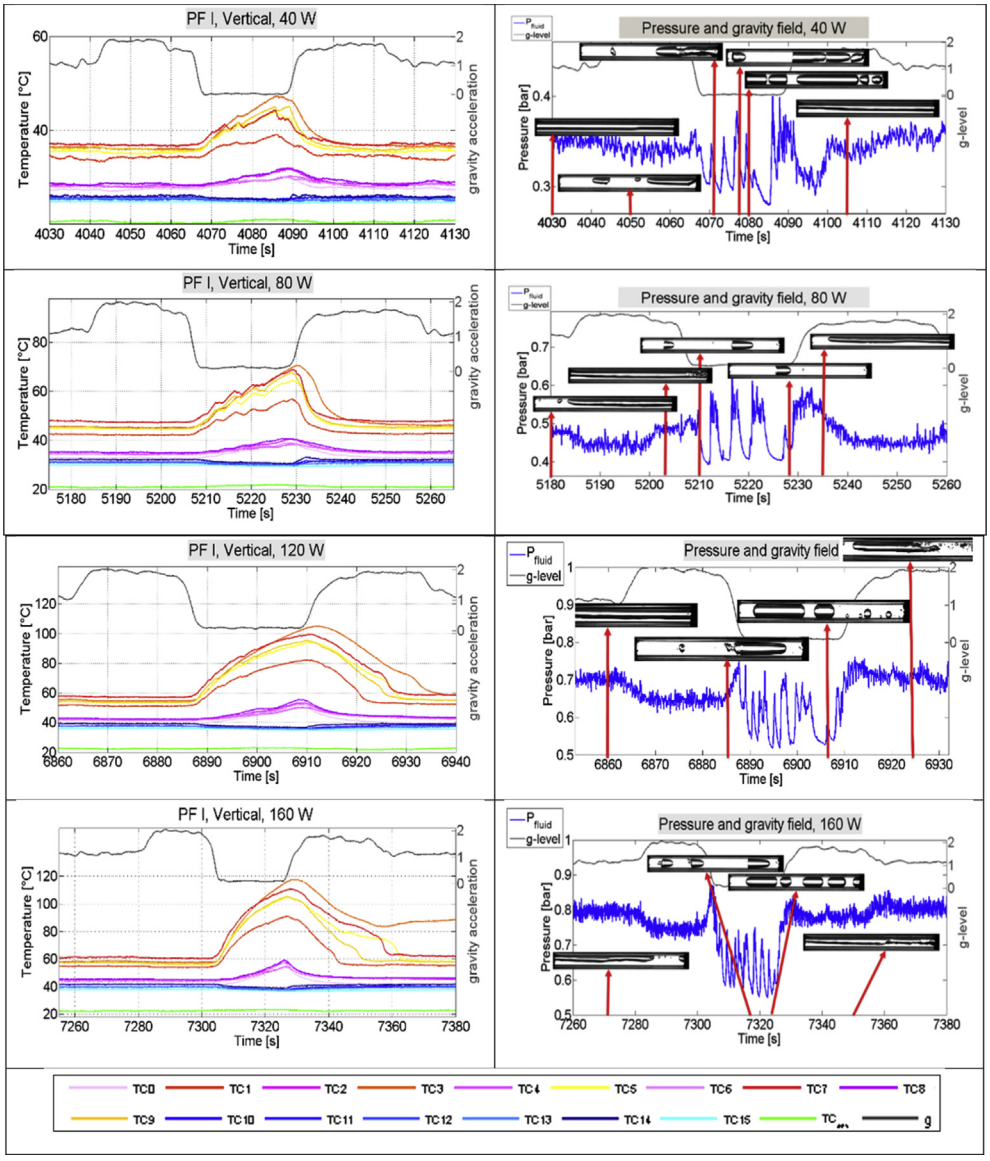

Fig. 6. (*continued*).

sides of the device respectively. As it can be observed from the sequence of images recorded at 100 Hz, in Fig. 5b, the leading edge of the vapor bubble points out a fluid motion from the right to the left, further confirming the net circulation in a preferential direction.

3.1.2. Horizontal orientation

When the device is positioned in the horizontal orientation, gravity is never assisting the fluid motion. Therefore, since the fluid is stratified and the whole vapor phase resides in the upper half of the tube, its expansion is not able to push the fluid and the device works practically as a purely conductive medium. The equivalent thermal resistance stabilizes to a constant value of approximately 0.7 K/W, since the motion of the fluid is not activated for all the heat power inputs tested. This confirms the importance of having a gravity head between the evaporator and the condenser zone for the Thermosyphon. Moreover, it was observed that temperatures increase as the heat power input increases (Fig. 4a) and the pressure measured in the condenser zone does not exhibit any fluctuation (Fig. 4b).

3.2. Flight tests

Microgravity experiments have been performed aboard the ESA/Novespace Airbus A300, during the 61st ESA PF campaign. A total of 31 parabolic trajectories are performed in each flight: the first one, called parabola zero, is followed by six sequences, each consisting of five consecutive parabolic maneuvers. All sequences are separated by 5 min interval at earth g-level. Each parabolic maneuver is itself subdivided into three parts: 20 s at 1.8 g (hyper-gravity), followed by 22 s at 0.01 g (micro-gravity) and finally 20–25 s at 1.8 g (hyper-gravity). A 90 s period of earth g-level is in between each parabolic event [16]. One flying day has been devoted to each of the two experiments summarized in Table 3, PF-I and PF-II respectively. Finally, the third day of the campaign is devoted to ensure the repeatability of the horizontal test, as will be explained more thoroughly in section 3.2.2. The heat input level is changed during the 5 min pause at normal g between each sequence, in order to reach the pseudo-steady state before the beginning of the parabolic trajectories (1 g, 1.8 g, 0 g, 1.8 g, 1 g). This procedure is followed in all of the six sequences, ensuring data repeatability.

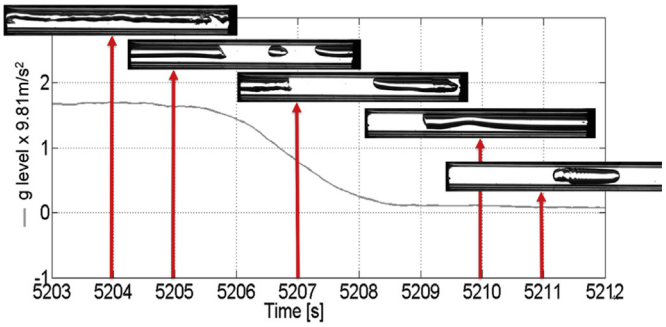

Fig. 7. Transition from the hyper-gravity period to the micro-gravity period: slug/plug flow activation.

3.2.1. Vertical orientation

Focusing on Fig. 6, it is possible to recognize the thermal response of the device during the gravity field variations. As shown previously, during the ground tests in vertical position, at 10 W and 20 W, the heat power is not sufficient to pump the liquid batches in the condenser zone. Therefore, during the parabolic flight experiments, the temperatures appear stable in the normal and the hyper-gravity conditions, the pressure does not show fluctuations and the transparent section remains dry. When the microgravity period starts, a slug/plug flow is observed in the transparent condenser section and the temperature values at the evaporator zone decrease rapidly. The liquid phase is indeed able to reach more easily the condenser zone when the body force becomes negligible during the microgravity period, and the slug/plug flow activation allows the fluid motion in the condenser zone, even for the lowest

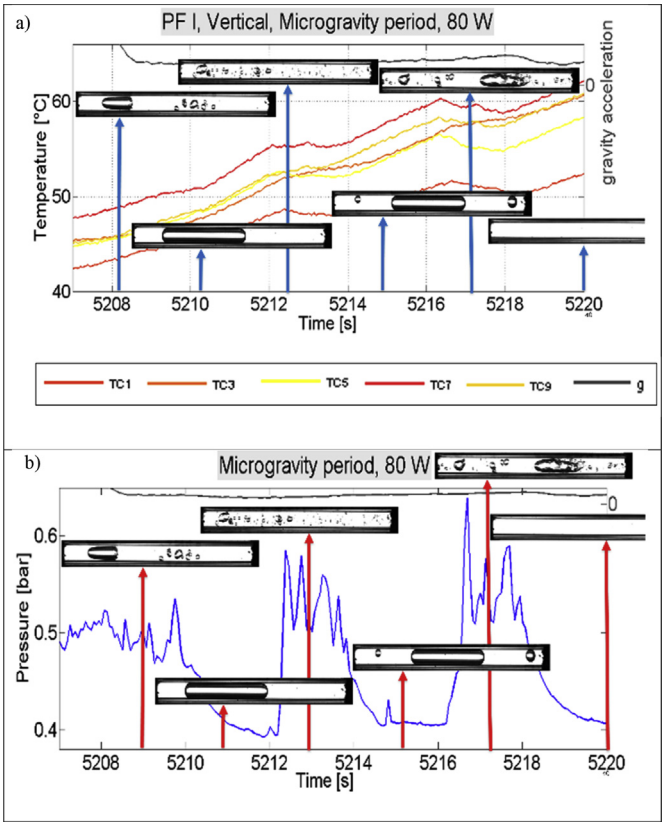

Fig. 8. Microgravity period at 80 W; a) temperatures recorded at the evaporator zone; b) pressure signal and images.

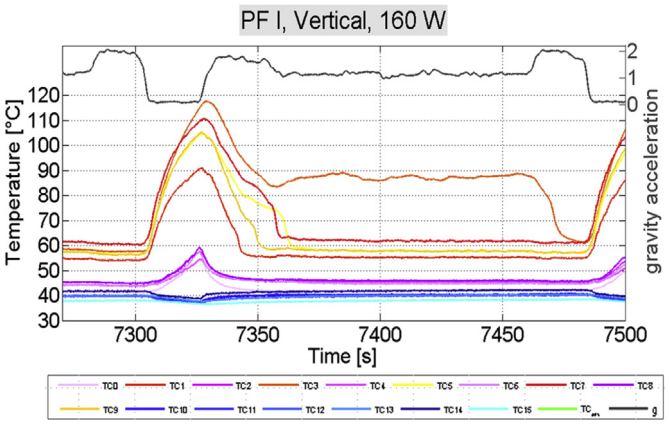

Fig. 9. Hyper-gravity effect on partial dry-out occurred at 160 W.

heat power input levels tested. For all the other heat power inputs tested, when the device reaches the standard operating conditions as TS, the gravity certainly assists the device, giving a net contribution to the fluid momentum. The beginning of microgravity, activating the slug/plug flow regime, makes the device to work as a PHP, increasing the temperatures at the evaporator zone and decreasing the thermal efficiency. Interestingly, the fluid motion does not stop completely in microgravity: the temperatures do not exhibit an ever-increasing trend, but the oscillating slug/plug flow motion, increasing the convection, tends to stabilize the temperatures.

The temporal evolution in Fig. 7, that focuses on the fluid dynamic between the hyper and micro-gravity transition, shows that during microgravity, the buoyancy forces become negligible and the surface tension of the liquid phase tends indeed to create liquid/vapor interfaces perpendicular to the flow path (i.e. menisci). Since the vapor phase fills completely the tube section, the flow pattern results in an alternation of vapor plugs and liquid slugs, enabling the device to start working as a PHP.

After the slug/plug flow regime activation, the fluid is no more circulating in a preferential direction, but it is characterized by pulsations (typical of a PHP) as shown in Fig. 8a, where fluid oscillation can be detected both from the pressure transducer readings as well as from the corresponding images. When the pressure is nearly constant, the fluid in the condenser zone is not moving, and the vapor plugs inside the transparent section of the condenser remain at the same position. Such short stop-over periods are followed by vigorous fluid pulsations with a positive impact on the heat exchange. Indeed, as soon as the fluid starts to oscillate in the condenser transparent section, an abrupt decrease of the evaporator temperatures is also recognizable, as shown in Fig. 8.

The beneficial effect of gravity, when the device works in TS mode, is recognizable at the highest heat power input tested (160 W). In some case for example, after a parabola, the temperature recorded by one thermocouple (TC3 in the example of Fig. 9) sets at approximately 90 °C, probably due to a partial dry-out. The next hyper-gravity period is able to eliminate such partial dry-out restoring the correct operation until the occurrence of the next microgravity period confirming the results obtained by Mameli et al. [17] on a capillary PHP tested in hypergravity conditions aboard ESA Large Diameter Centrifuge.

3.2.2. Horizontal orientation

During microgravity, the inclination of the device does not play a significant role because of the complete absence of the body

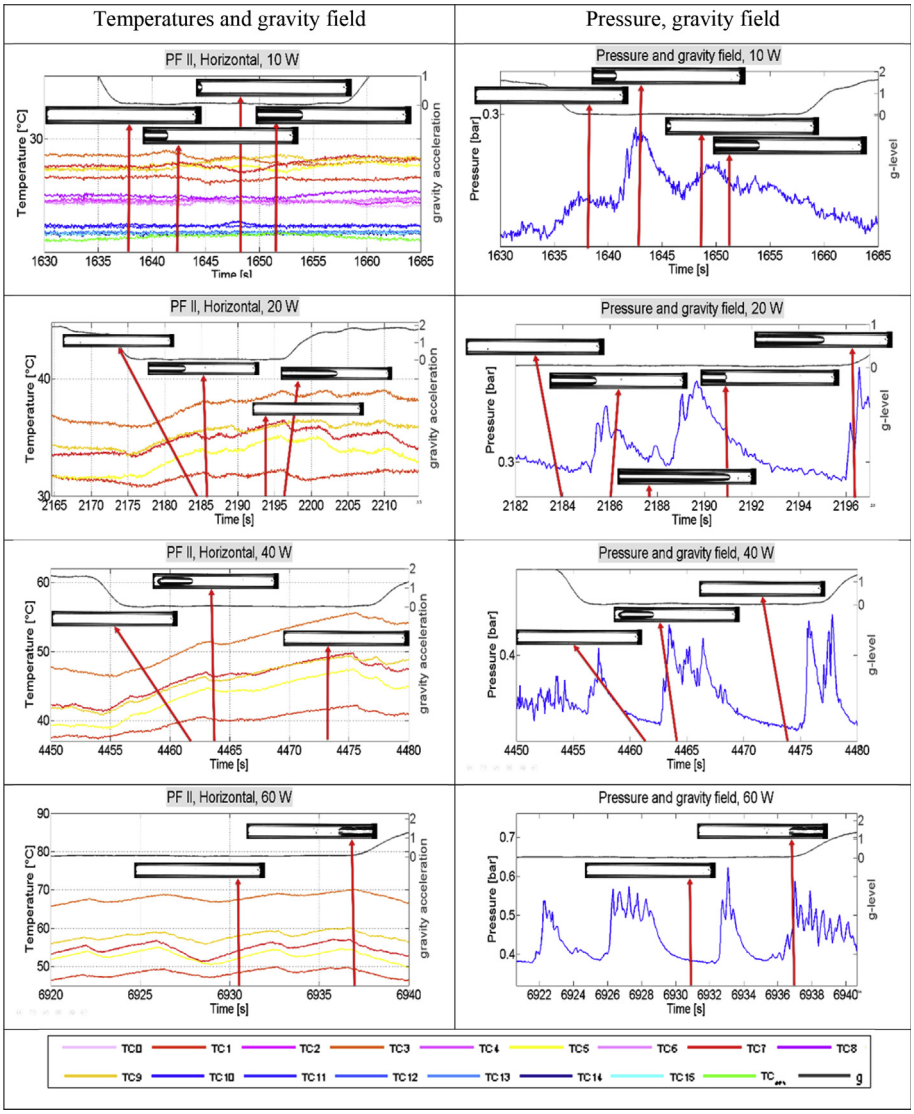

Fig. 10. Microgravity period for different heat inputs tested in horizontal orientation; first column: evaporator temperatures, gravity field and images; second column: pressure, gravity field and images.

force: the temperatures and the pressure measurements are similar to the microgravity case during the BHM test (PF-I). The vapor plugs, generated during the absence of gravity field, are similar to a piston that pumps the liquid columns through the condenser, due to their expansion in the evaporator section. This kind of fluid motion is of course beneficial for the thermal performance of the device: as soon as the slug/plug flow is activated, the evaporator temperatures start to oscillate, as it is depicted in the second column of Fig. 10. This is however not possible in the normal gravity condition, since the liquid phase fills completely the lowest half part of the tube, and there is no possibility to pump the flow in the condenser zone (see Fig. 4).

Carefully observing Fig. 10, it can be noticed that the fluid motion is often activated during the first hypergravity period, causing a sudden decrease in the evaporator temperatures. However, this is not occurring during the second hyper-gravity period.

This can be explained observing the acceleration components plotted in Fig. 11. It is obvious, that the proposed activation is not due to the acceleration in the z-direction, but to the "spurious" force in the x direction (green line (in the web version) in Fig. 11b). During the first hypergravity period due to g_x component orientation the generated inertia force causes the fluid to move in the opposite direction, improving the beneficial effect due to the thermal asymmetry. However, during the second hypergravity period, g_x is negative inhibiting this preferential fluid motion.

This also affects the upcoming microgravity period: evaporator temperatures are decreasing during the first hypergravity period (Fig. 11c) since the fluid is already moving inside the device as witnessed by the fluid oscillations recorded by the pressure transducer (Fig. 11d). However, it should be mentioned that during micro-gravity all the gravity vector components are close to zero, therefore, the fluid motion is mainly due to the slug/plug motion. Summarizing, the parabolic flight tests have demonstrated that a transition from the Thermosyphon to the PHP working modes occurs during the microgravity periods.

4. Conclusions

A novel concept of hybrid Thermosyphon/Pulsating Heat Pipe with a diameter bigger than the static threshold level on ground and around the dynamic threshold level in microgravity conditions (I.D. of 3 mm filled with FC-72) is tested both on ground and in

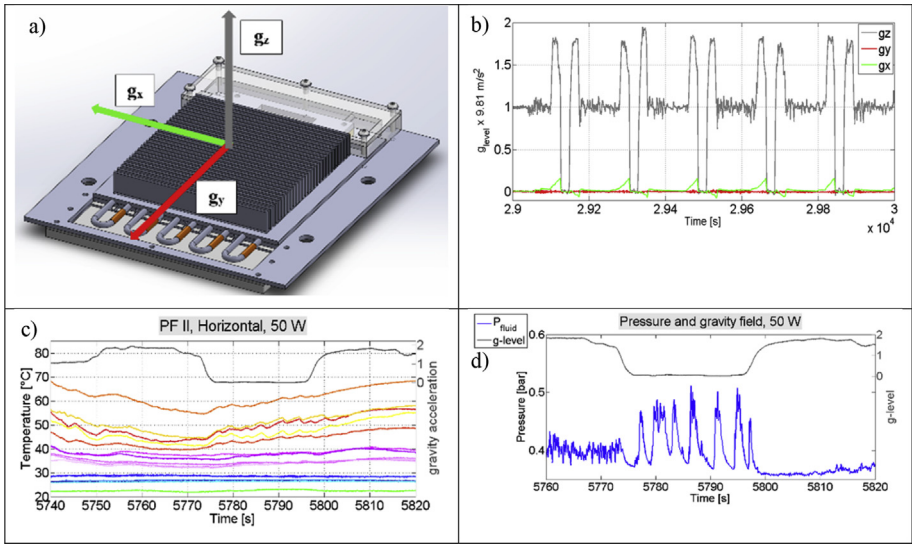

Fig. 11. g_x, g_y, g_z acceleration components and time evolution during parabolic maneuvers in horizontal orientation: a) Layout and directions; b) g_x, g_y, g_z acceleration over time; c) effect on temperatures; d) effect on fluid pressure.

hyper/micro gravity conditions during the 61st ESA Parabolic Flight Campaign. According to the authors' best knowledge, this is the first attempt in literature that such a hybrid device is tested. The device is made with an aluminum tube, equipped with 16 thermocouples (10 at the evaporator zone, 6 in the condenser zone) and with a pressure transducer in the condenser zone. Moreover, a glass tube (50 mm of axial length) closes the loop in the condenser zone, allowing also fluid dynamic visualization during gravity field variations. The temporal trend of the wall temperature, the local fluid pressure in the condenser zone together with images recorded at 450 fps in the transparent section of the condenser zone, indicate that the device performance is strongly affected by the variation of the gravity field. In particular, the following salient points are raised:

- The device on ground works as a Closed Loop Two Phase Thermosyphon, where the fluid circulation is activated at high heat input levels thanks to the asymmetric location of the heating sections reaching an equivalent thermal resistance of 0.1 K/W with heat fluxes up to 17 W/cm^2.
- The ground test in horizontal orientation points out that the device works as a pure conductive medium. No fluid motion is recognized, remarking the importance of a gravity head between the evaporator one and the condenser zone during the TS mode.
- The parabolic flight tests reveal that the device operates in a complete different way when the microgravity is reached: the images recorded in the condenser zone, together with the pressure signal shows a transition from the Thermosyphon mode to the PHP working mode.
- The flight test in vertical position points out a start-up also at the lowest heat power input levels in microgravity. The vapor plugs, expanding in the evaporator zone, permits to the adjacent liquid column to reach the condenser zone, promoting the heat exchange also at 10 W and 20.
- During microgravity, a slug/plug pulsating flow is observed also when the PHP is in the horizontal position.
- In some cases the hyper-gravity period is able to eliminate partial dry-outs restoring the correct operation until the occurrence of the next microgravity period.

Acknowledgments

The present work has been carried out in the framework of the Italian Space Agency (ASI) project ESA_AO-2009 entitled “Innovative two-phase thermal control for the International Space Station”. The authors would like to thank the NOVESPACE team in Bordeaux as well as to Dr. Vladimir Pletser for their support and encouragement during the parabolic flight campaign. The authors would like to thank Dr. Olivier Minster and Dr. Balazs Toth for their interest and support to the PHP activities and for the fruitful discussions. Also we acknowledge Ing. Paolo Emilio Battaglia of the Italian Space Agency for his administrative support. Finally we thank all the members of the Pulsating Heat Pipe International Scientific Team, led by Prof. Marco Marengo, for their contribution in pushing the PHP technology for space applications, with a particular gratitude to Prof. Sameer Khandekar, Dr. Vadim Nikolayev and Dr. Vincent Ayel.

References

[1] G. Gilmore, Spacecraft Thermal Control Handbook, in: Fundamental Technologies, vol. 1, The Aerospace Press, El Segundo California, 2002.
[2] H. Akachi, Structure of a heat pipe. US Patent 4,921,041, 1990.
[3] M. Mameli, M. Marengo, S. Khandekar, Local heat transfer measurement and thermo-fluid characterization of a pulsating heat pipe, J. Therm. Sci. 75 (2014) 140–152.
[4] H. Yang, S. Khandekar, M. Groll, Operational limit of closed loop pulsating heat pipes, Appl. Therm. Eng. 28 (1) (2008) 49–59.
[5] C. Baldassari, M. Marengo, Flow boiling in microchannels and microgravity, Prog. Energy Combust. Sci. 39 (1) (2013) 1–36.
[6] J. Qu, H. Wu, P. Cheng, Start-up, heat transfer and flow characteristics of silicon-based micro pulsating heat pipes, Int. J. Heat Mass Transf. 55 (2012) 6109–6120.
[7] M. Mameli, V. Manno, S. Filippeschi, M. Marengo, Thermal instability of a closed loop pulsating heat pipe: combined effect of orientation and filling ratio, Exp. Therm. Fluid Sci. 59 (2014) 222–229.
[8] S.M. Thompson, P. Cheng, H. Ma, An experimental investigation of a three-dimensional flat-plate oscillating heat pipe with staggered microchannels, Int. J. Heat Mass Transf. 54 (2011) 3951–3959.
[9] Y. Maydanik, V.I. Dmitrin, V.G. Pastukhov, Compact cooler for electronics on the basis of a pulsating heat pipe, Appl. Therm. Eng. 29 (2009) 3511–3517.
[10] J. Gu, M. Kawaji, R. Futamata, Effects of gravity on the performance of pulsating heat pipes, J. Thermophys. Heat. Transf. 18 (3) (2004) 370–378.
[11] J. Gu, M. Kawaji, R. Futamata, Microgravity performance of micro pulsating heat pipe, Microgravity Sci. Technol. 16 (2005) 181–185.

[12] K.V. Paiva, M.B.H. Mantelli, L.K. Slongo, Experimental tests of wire mini heat pipe under microgravity conditions aboard suborbital rockets, in: 9th IHPS, Malaysia, Nov. 2008.
[13] M. Mameli, L. Araneo, S. Filippeschi, L. Marelli, R. Testa, M. Marengo, Thermal response of a closed loop pulsating heat pipe under a variable gravity force, Int. J. Therm. Sci. 80 (2014) 11–22, http://dx.doi.org/10.1016/j.ijthermalsci.2014.01.023.
[14] C.D. Henry, J. Kim, B. Chamberlain, Heater size and heater aspect ratio effects on sub-cooled pool boiling heat transfer in low-g, in: 3rd International Symposium on Two-Phase Flow Modeling and Experimentation Pisa, 22–24 September 2004.
[15] A. Franco, S. Filippeschi, Closed loop two phase thermosyphon of small dimensions: a review of the experimental results, Microgravity Sci. Technol. 24 (2012) 165–179, http://dx.doi.org/10.1007/s12217-011-9281-6.
[16] Novespace A300 Zero-G Rules and Guidelines, RG-2009-2, April, 7th 2009, NOVESPACE 15, rue des Halles 75001 Paris, France.
[17] M. Mameli, M. Manzoni, S. Filippeschi, L. Araneo, M. Marengo, Experimental investigation on a closed loop pulsating heat pipe in hyper-gravity conditions, in: 15th International Heat Transfer Conference, Kyoto, 10-15 August, 2014.